

Second-harmonic imaging of ferroelectric domains in LiNbO₃ with micron resolution in lateral and axial directions

M. Flörshheimer^{1,*}, R. Paschotta^{2,**}, U. Kubitscheck³, Ch. Brillert¹, D. Hofmann², L. Heuer², G. Schreiber², C. Verbeek³, W. Sohler², H. Fuchs¹

¹Physical Institute, University of Münster, D-48149 Münster, Germany
 (Fax: +49-251/83-33602, E-mail: florshl@nwz.uni-muenster.de)

²Applied Physics, University of Paderborn, D-33098 Paderborn, Germany
 (Fax: +49-5251/60-3422, E-mail: Sohler@physik.uni-paderborn.de)

³Institute for Medical Physics and Biophysics, University of Münster, D-48149 Münster, Germany
 (Fax: +49-251/83-55121, E-mail: kubitsc@uni-muenster.de)

Received: 22 May 1998/Revised version: 10 July 1998

Abstract. We demonstrate that scanning second-harmonic microscopy with a mode-locked laser can be used as a non-destructive technique to image ferroelectric domain structures with micron resolution in both lateral and axial directions. This method is expected to have significant impact particularly on the further development of nonlinear optical bulk and waveguide devices with periodically poled ferroelectric crystals.

PACS: 07.60.Pb; 42.30; 77.80.Dj

Ferroelectrics such as LiNbO₃, KNbO₃, or BaTiO₃ play an important role in nonlinear optics and electro-optics because of their large second-order nonlinearities. A ferroelectric crystal may be composed of domains with different polar orientations. LiNbO₃, for example, whose crystal symmetry is $3m$, can show two different domain orientations. They differ in the signs of all non-vanishing components of the nonlinear optical tensor $\chi^{(2)}$. Hence, for nonlinear optical experiments and applications, it is crucial to control the domain structure of the crystals.

Devices for holographic data storage and optical parallel processing [1, 2] or for nonlinear frequency conversion with birefringent phase-matching usually require crystals with a single domain, whereas in recent years a lot of interest has been attracted by crystals fabricated with a periodic domain structure, mainly for quasi-phase-matched frequency conversion [3, 4]. The technique of quasi-phase-matching (QPM) opens a number of very attractive possibilities in nonlinear optics: virtually any nonlinear interaction of waves within the transparency region of the crystal can be noncritically phase-matched at room temperature, and in addition QPM devices can be significantly less sensitive to the photorefractive effect [5], which is particularly important for the generation of visible light. The crucial prerequisite

for using QPM is the ability to fabricate crystals with periodic domain structures of good quality, typically with periods in the range from 3 μm to 30 μm . Various techniques have been used for this purpose, most successfully the technique of electric-field poling [6–8]. In any case, the further development of such methods requires techniques for the characterization of the obtained domain structures. First we briefly review the currently available techniques and later describe our new technique which is non-destructive, reproducible, quick and versatile, and provides images of domain structures with micron resolution in both lateral and axial directions.

1 Alternative techniques for the observation of ferroelectric domains

Polarization microscopy is well suitable for the observation of the anisotropic grains in polycrystalline matter. The linear optical technique, however, does not allow us to distinguish between the antiparallel domains in ferroelectrics. Domain boundaries can cause visible structures due to stress birefringence or due to the electro-optic effect originating from charges on the boundaries. The unambiguous identification of domain structures, however, seems not to be possible with this method.

Selective etching can be used to transform the domain structure on the surface of a crystal into a topographic structure [9, 10] that can be observed with a usual microscope. This method, however, is destructive, provides information about the domain structure on a polished surface but not from the interior of the specimen, and it works only on certain crystal faces (for example, on the Y and Z face, but not on the X face of a LiNbO₃ crystal). Another method applied to crystal surfaces is the deposition of electrically charged powder particles [11]. This technique is non-destructive but suffers from a poor accuracy of the obtained images. Other non-destructive techniques such as atomic force microscopy [12–14] and scanning secondary-electron microscopy [15, 16] have recently been applied to ferroelectric crystal surfaces. However, they also do not provide information on the interior domain structure. X-ray topography studies can reveal strain,

* To whom correspondence should be addressed

** Present address: Institute of Quantum Electronics, Swiss Federal Institute of Technology, ETH-Hönggerberg, HPT E 17, CH-8093 Zürich, Switzerland, Phone: +41-1/633-6825, Fax: +41-1/633-1059, E-mail: paschott@iqe.phys.ethz.ch

lattice dilations, and defects induced by domain reversal [17], but with no depth resolution. Three-dimensional images of the domains inside a crystal have been obtained with photorefractive beam coupling [18–20], but this method provides limited resolution and is applicable only to photorefractive materials.

Second-harmonic (SH) microscopy is another possibility to observe antiparallel domains. Recently, Kurimura and Uesu illuminated ferroelectric crystals with an almost parallel laser beam in a transmitted light geometry [21]. The SH light radiated in the forward direction was used to image the exit face of the crystal with a stigmatic (non-scanning) linear optical polarization microscope. Contributions to the SH light were generated in the whole crystal along the beam path. Inverted domains situated below the surface could be clearly observed and distinguished from the neighboring undisturbed regions because the contribution of the inverted crystal parts to the total SH signal had a different phase as compared with the noninverted parts. Stigmatic imaging, however, can hardly provide depth resolution.

Independently, we have built a similar *stigmatic SH microscope* for the imaging of *surfaces* or *interfaces*. At the surface of a centrosymmetric substrate [22], an SH signal can be generated that is specific to the symmetry and order of the surface. We have used this signal for the quick, quantitative characterization of surfaces [23, 24]. We have also applied this microscope to the investigation of noncentrosymmetric bulk samples such as LiNbO_3 and obtained a contrast between domains in the same way as described above [25]. The lateral resolution limit is Abbe's resolution for the SH light with a wavelength of 532 nm in our case, but the signal contains contributions from the whole depth of the crystal.

Among all these different techniques there was still not a single one which allows us to image non-destructively the domain structure in the interior of a sample with a micron resolution. Below, we demonstrate that we have now achieved this goal. High axial and lateral resolution is obtained simultaneously by three-dimensional *scanning* of the sample with a *tightly focused high-power* laser beam. This method is a modification of a second-order nonlinear optical technique [26–28] that is widely applied for the investigation of biological and medical specimens. In these studies, the sample is usually stained with a fluorescent dye. Due to the high light intensity in the laser focus, the fluorescence of the dye can be excited through two-photon absorption. The two-photon fluorescence intensity depends quadratically on the laser intensity. As a result, the nonlinear optical signal is dominated by contributions from the *center* of the laser spot which allows a high axial and lateral resolution [29].

If structural details of the specimen are noncentrosymmetric, SH light can be generated at these structural features and staining is not required. SH imaging using a high-power scanning microscope can provide comparable resolution as in the case of two-photon fluorescence scanning microscopy. Scanning SH microscopy was previously applied to study the polar order of rattail tendon [30] and to image inhomogeneities in nonlinear optical crystals [31]. To our knowledge, however, this technique was not applied to investigate the domain structure of ferroelectrics systematically. In fact, it is not obvious that antiparallel domains should be visible in this way: if the tightly focused laser beam generates SH light within one domain of a material such as LiNbO_3 , the SH power should

not depend on the polarity of the domain. However, we have obtained bright lines showing the domain boundaries with almost diffraction-limited resolution. The only disadvantage as compared with techniques such as selective etching or photorefractive beam coupling is that we could not determine the sign of the domains' polar orientation. We first describe the experimental details of our microscope in Sect. 2, then in Sect. 3 the geometry of the samples investigated, and in Sect. 4 the observations made. Finally in Sect. 5, we attempt an explanation for the success of this novel method of characterizing ferroelectric domain structures.

2 The microscope and its resolution

For the experiments, a laser scanning microscope (LSM 410, Carl Zeiss, Jena, Germany) equipped with an oil immersion objective (40 \times , numerical aperture 1.3) was applied. The microscope was modified to make it suitable for SH generation and detection by using a pulsed Ti:sapphire laser (Tsunami, Spectra Physics, Darmstadt, Germany) and suitable dichroic and detection filters. The Ti:sapphire laser was pumped by a frequency-doubled Nd:YAG laser (5 W Millennia, Spectra Physics). The pulse repetition rate of the Ti:sapphire laser was 82 MHz, the pulse duration 80 fs, and the average output power 500 mW at a wavelength of 820 nm. This corresponds to a peak power of 67 kW assuming a sech^2 pulse shape. The power losses between the laser and the sample amounted to $\approx 95\%$, such that the average power at the sample was ≈ 25 mW. Over-illumination of the objective's entrance pupil caused the input laser beam to be focused down to the smallest possible size. The focal spot was scanned linewise across the object plane by means of galvanometer mirrors. The axial position of the focus within the sample could be altered by an axial motion of the stage that supported the sample.

The light intensity in the laser spot was high, its exact value, however, can only be estimated due to several reasons. Group velocity dispersion in the optical system of the microscope and chromatic aberrations due to the refractive index mismatch between immersion oil and the LiNbO_3 sample determine the actual focus shape and pulse length in the sample [32]. Assuming a pulse duration of 300 fs in the sample, and a full width at half maximum (FWHM) diameter of the illuminated spot of 360 nm (see below), the peak irradiance is estimated to be 4.5×10^{11} W/cm². In some experiments, attenuation filters (transmission of 10% or 30%) were used.

Images could be obtained operating the microscope in the transmitted- or in the reflected-light mode. The contrast in the latter geometry, however, was superior as compared with the former mode. Thus, the images shown here were taken in the reflected-light geometry. The backward-scattered fundamental and frequency-doubled light were collected by the objective. Then, they were spectrally separated using a dichroic beamsplitter (670 nm, Carl Zeiss, Jena, Germany) and a short-pass filter (650 nm, Laser Components, Olching, Germany) for the SH light. Finally, the SH signal was measured as a function of the spot position using a photomultiplier. For various samples, the measured signal was proved to depend quadratically on the laser intensity as expected for SH generation. For these measurements, the fundamental intensity was reduced applying calibrated neutral density filters.

The recording time required for an image of the LiNbO₃ samples with 512 × 512 pixels was of the order of 1 s.

The optical resolution of the modified laser scanning microscope was investigated by two-photon excitation of fluorescein-labelled latex beads (diameter 170 nm, Polysciences, Eppelheim, Germany). The beads were immobilized in a 30% polyacrylamide gel with a refractive index of 1.39 [33]. The two-photon fluorescence signal from the beads detected in the wavelength range from 500–600 nm was used for imaging. In images from sections perpendicular to the optical axis, the beads appeared with an FWHM diameter of (360 ± 20) nm. This value can be used as an estimate of the lateral resolution. The axial resolution was determined by scanning the specimen along the optical axis. The thus determined axial intensity profile displayed an FWHM of (1 040 ± 50) nm. The resolution can further be improved by using a confocal pinhole in the detection beam path. Confocal detection, however, was not applied here.

Depth measurements by scanning microscopy using an immersion lens are impaired due to a mismatch of the immersion oil refractive index n_0 and the respective sample refractive index n_i . This mismatch shows a twofold effect. At first, the axial movement Δs of the scanning stage does not directly correspond to the movement Δf of the focus position in the sample. Secondly, the shapes of the illumination intensity and detection probability profiles are altered resulting in a depth-dependent increasing loss of resolution. These two effects can be calculated using a quasi-vectorial theory of light [34]. The relationship between Δs and Δf is linear in good approximation up to a depth of a few 10 μm . For the polyacrylamide gel ($n_1 = 1.39$, $n_0 = 1.518$), we calculated $\Delta f = 0.84\Delta s$. Describing LiNbO₃ with an isotropic refractive index of $n_2 = 2.30$, we obtained $\Delta f = 1.63\Delta s$. For the axial FWHM resolution in the gel, we calculated 620 nm at a depth of 5 μm , a fundamental wavelength of 820 nm, and a fluorescence wavelength of 410 nm. The measured axial FWHM of the signal profile [(1 040 ± 50) nm] corrected by the factor of 0.84 leads to an axial resolution of (870 ± 40) nm. This value is somewhat larger than the theoretical result. The superior theoretical resolution, however, seems reasonable because the calculation describes an ideal case with a perfectly planar incoming wavefront. The lateral resolution in the gel was calculated to be 310 nm, which is also somewhat better than the experimental result [(360 ± 20) nm]. Using the same theoretical approach we calculated the axial and lateral resolution for two-photon fluorescence microscopy in a material with the refractive index of LiNbO₃. The results are 1370 nm and 250 nm, respectively, for a depth of 5 μm .

3 Description of the samples

The geometry of the samples, all consisting of LiNbO₃, is shown schematically in Fig. 1. The crystallographic axes (X , Y , and Z) are indicated in each case. Figure 1a shows the geometry of sample A, a bulk periodically poled specimen. It was a Z -cut wafer produced and poled by Crystal Technology, Inc., with a period of $\approx 30 \mu\text{m}$. We also polished the X face of this sample. Specimen B, shown in Fig. 1b, exhibits a 24- μm -wide and 3- μm -high ridge, fabricated by ion beam etching on the $-X$ face of an X -cut sample. An opti-

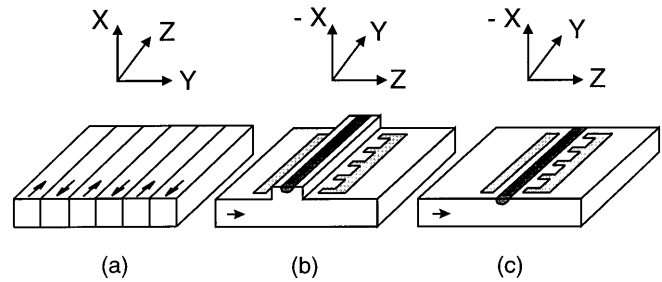


Fig. 1a–c. Geometry of the investigated specimens. The crystallographic axes (x , y , z) are indicated. **a** Bulk specimen A from Crystal Technology, Inc., periodically poled. The *arrows* in the domains correspond to the local polar axes. **b** Sample B with a ridge, a titanium-indiffused waveguide on the ridge, and electrodes as used for periodic poling of regions in the ridge. (The periodic domain structure is not shown.) **c** Sample C, similar to sample B, but without ridge. In the experiments, the specimens were observed from the X side (**a**) or from the $-X$ side (**b,c**)

cal waveguide represented as a dark stripe on the ridge was fabricated by titanium indiffusion. The aluminium electrodes (period $\approx 17 \mu\text{m}$) shown in Fig. 1b (shaded) were used for periodic poling with an electric field but were removed after the poling process. Figure 1c shows sample C. It is similar to sample B but the waveguide is in a plane surface without a ridge.

4 Results and comparison with information obtained from selective etching

SH micrographs of the samples A, B, and C are given in the Figs. 2, 3, and 4, respectively. The specimens were observed from the top side as shown in Fig. 1 (X or $-X$ side). The pump light was polarized in the direction of the crystal z axis which corresponds to the vertical direction in all images. This polarization resulted in the strongest signal as expected because d_{33} is the largest nonlinear tensor component in LiNbO₃. The SH light was always detected without prior polarization filtering. The grey scale of all the SH micrographs is a measure of the square root $\sqrt{I^{(2\omega)}}$ of the SH intensity ($\sqrt{I^{(2\omega)}} \propto d_{\text{eff}}$) with d_{eff} the effective susceptibility of the specimen). Using such a scale, all the different phenomena in the images can be well observed. In contrast, the lower intensity phenomena disappear in the background if using the original code that is linear in the SH intensity. The images were not further processed or improved.

Figure 2a was taken with the focus of the laser near the sample surface ($s = 0$, $f = 0$) whereas Fig. 2b was obtained with the focal plane at a depth of $f = -3.3 \mu\text{m}$. The grey code of the two images is identical. They can be directly compared. Sharp, vertical stripes are observed with a different SH intensity compared to the background. The average distance between the stripes is half a domain period. Obviously, the stripes indicate domain walls with some deviation from perfect periodicity. Also, an SH signal is detected from the surface of the domains (see Fig. 2a), which is stronger than the signal from the regions below the surface (Fig. 2b). The variation of the SH intensity over the surface in Fig. 2a is mostly due to non-perfect horizontal alignment of the crystal. Various images have been taken up to a depth of $f = -11 \mu\text{m}$ below the surface. They all look very similar to Fig. 2b. The

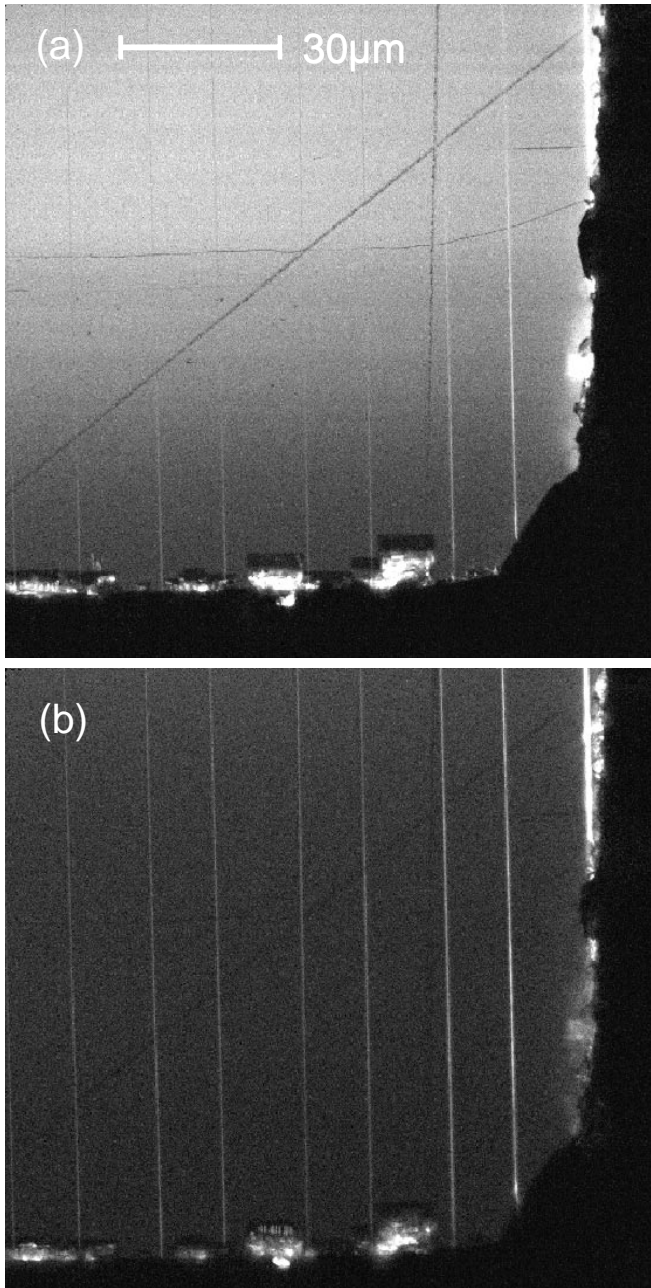


Fig. 2a,b. Second-harmonic images of a polished X face of sample A, taken from the surface ($s = 0$, $f = 0$) (a) and from a section through the bulk of the specimen at $f = -3.3 \mu\text{m}$ (b). The period of the domain walls (vertical lines) is $\approx 30 \mu\text{m}$

lateral width (FWHM) of the intensity profile through the domain walls is $(400 \pm 100) \text{ nm}$.

Figure 3 shows three images of sample B. Figure 3a was obtained at the level of the ridge's surface ($s = 0$, $f = 0$). For the image of Fig. 3b, the distance between the sample and the objective was reduced by $2.0 \mu\text{m}$ ($s = -2.0 \mu\text{m}$). Beside the ridge, the laser focus is thus $1 \mu\text{m}$ above the sample surface. Below the ridge, a section at a depth of $f = -3.3 \mu\text{m}$ is imaged. Figure 3c was taken at $s = -3.0 \mu\text{m}$, which corresponds to the level of the surface beside the ridge. Below the ridge, Fig. 3c shows a section at $f = -4.9 \mu\text{m}$. In Fig. 3a and 3c, the uniform background SH signal from the surface

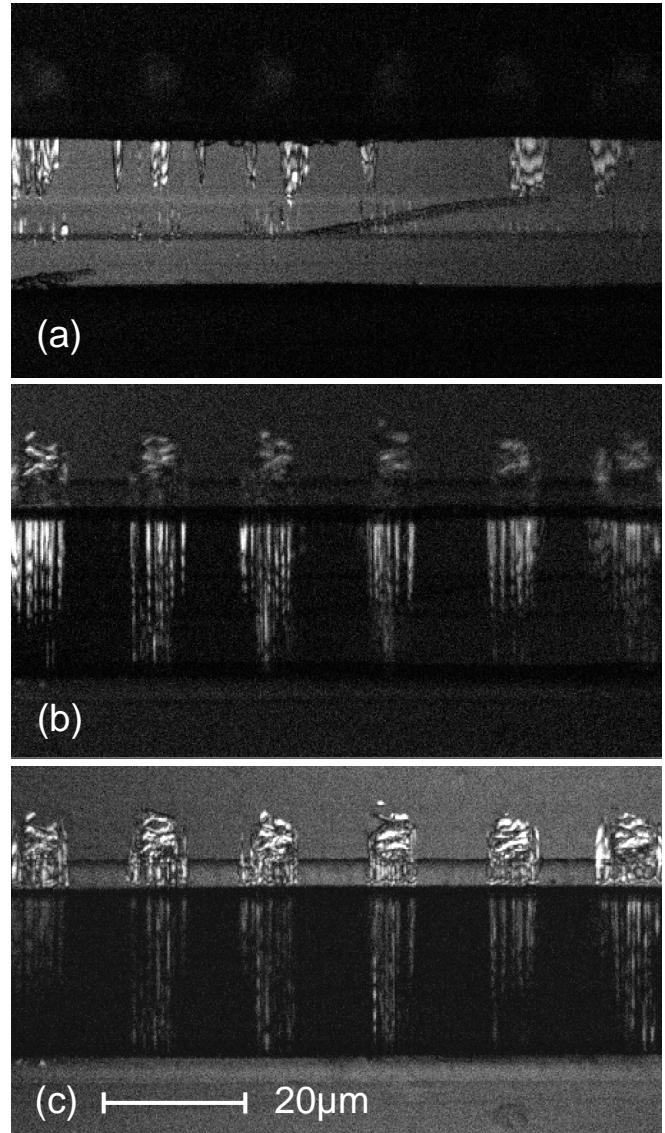


Fig. 3a–c. Second-harmonic images of sample B. **a** $s = 0$, $f = 0$ (focus of laser beam at surface level of the ridge). **b** $s = -2.0 \mu\text{m}$ (focus level $f = -3.3 \mu\text{m}$ below the ridge). **c** $s = -3.0 \mu\text{m}$ (focus level $f = 0$ at surface beside the ridge, $f = -4.9 \mu\text{m}$ below the ridge)

can be seen as described above for sample A. The indiffused waveguide can also be observed in Fig. 3a. Bright filaments oriented parallel to the z axis are visible in all images up to a depth of about $f \approx -5.5 \mu\text{m}$. Most of the filaments exhibit a small diameter. The smallest filaments' intensity profile shows a lateral width of $(400 \pm 100) \text{ nm}$. Their axial width, corrected with the factor of 1.63 for the refractive index mismatch (see Sect. 2), is $(1800 \pm 200) \text{ nm}$. The axial width of the surface signal which does not need to be corrected is $(1000 \pm 200) \text{ nm}$. The filaments correspond to the walls of the inverted ferroelectric domains as will be shown below.

In Fig. 3b and 3c, also bright spots of irregular structure are seen on the surface next to the ridge, just where the positive electrodes for the poling process were located. The application of high voltage to these electrodes and the following wet etching process has apparently damaged a part of the surface below the electrodes. Moreover, in Fig. 3a, areas with

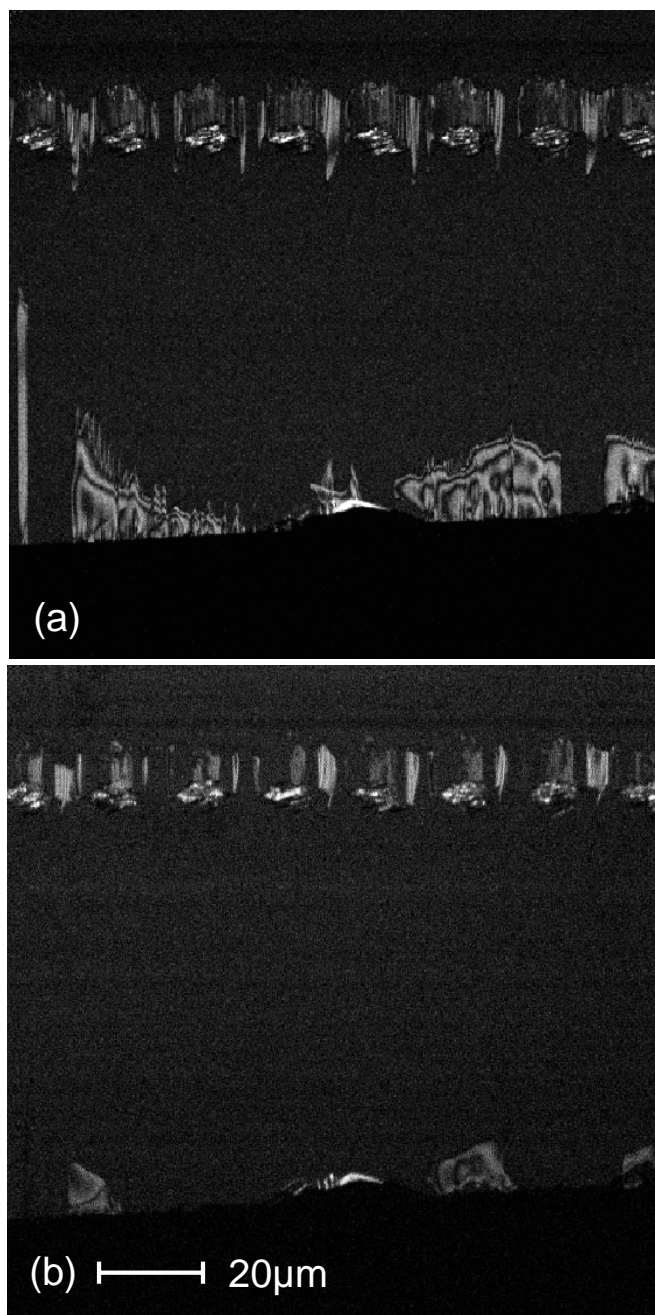


Fig. 4a,b. Second-harmonic micrograph of sample C. The sample had been heated to 500 °C (a) and 700 °C (b) for 1 h. Mechanical stress at the sawn border can be annealed at 700 °C. The filaments, however, are only marginally affected at this temperature indicating that the SH signal from the filaments is not due to stress

fringe patterns of unclear origin, apparently caused by some interference effects, can be seen.

We also investigated the change of the observed structures upon annealing at elevated temperatures. Figure 4a shows the polished $-X$ face of sample C after heating to 500 °C for 1 h. In this image, some structures are visible near the sawn edge of the sample. In another region of the image, filaments can be observed and spots at the positions of removed electrodes similar to those in Figs. 3b and 3c. The same specimen as in Fig. 4a is shown in Fig. 4b after annealing at 700 °C for 1 h.

The two images were taken with the focus of the laser beam at the sample surface.

The structures near the edge of the specimen in Fig. 4a were apparently caused by mechanical stress during the sawing of the crystal. These structures could not be seen under a linear optical polarization microscope. The filaments in Fig. 4a are oriented roughly parallel to the z axis just as the filaments in Fig. 3. In contrast to Fig. 3, the filaments in Fig. 4a are, however, not only located in the areas adjacent to the spots that come from the electrodes. The filaments of sample C exist also in the sections between the spots. In Fig. 4b, the structures at the border of the sample disappeared almost completely whereas the filaments and the spots are only slightly modified. The lateral width through the intensity profile of the smallest filaments of sample C is (400 ± 100) nm. At 800 °C, the filaments disappeared (not shown here).

In order to compare the SH micrographs with results from a traditional characterization method for poled ferroelectrics, we cut a type-B sample (Fig. 1b) normal to the z axis within a region that contained poled domains. The $-Z$ face of the crystal was then polished. By subsequent selective etching, the undisturbed crystal surface was attacked faster as compared with the inversely poled domains. The resulting topographic profile was transformed into a linear optical polarization microscopy contrast as depicted in Fig. 5. This image shows a cross section through a large number of inversely poled filaments with different diameters. The filament-like shape of the inverted domains is clearly unwanted. We have observed such structures only in samples with titanium-diffused waveguides. In the meantime, we have applied the SH imaging technique to find poling conditions for improved domain shapes. Thus, we have learned that much better shapes can be achieved by poling at elevated temperatures (for example at 200 °C). The triangular patterns in Fig. 5 reveal lattice defects in the titanium-diffused region.

Obviously, the filaments in the SH micrograph (Fig. 3) correspond to the poled filaments revealed by selective etching (Fig. 5). Precisely speaking, we think that the structures visible in the SH images are actually caused by the *surfaces of the poled filaments* because in sample A (Fig. 2), we also observed signals from the domain *walls*. The lateral width of the signal profile from the domain surfaces is (400 ± 100) nm in all the SH images. The coincidence of these data and their

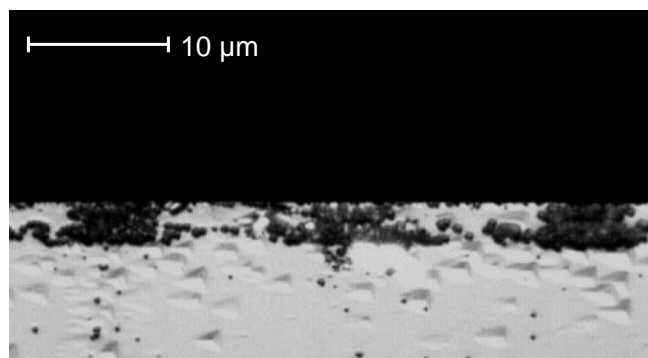


Fig. 5. Linear optical polarization micrograph of a type-B sample (Fig. 1b), polished through a periodically poled region ($-Z$ face) and selectively etched. A contrast between the $-Z$ face and the inverted domains is obtained. The walls of the filament-like domains correspond to the filaments revealed by second-harmonic microscopy

correspondence to the lateral resolution of the microscope as estimated with the fluorescent beads [(360 ± 20) nm, see Sect. 1] indicate that the actual width of the SH light source is below 400 nm. It can be concluded that the inverted domains (Figs. 3 and 4) whose diameter is significantly smaller than 400 nm appear with a resolution-limited lateral width of their intensity profile in the SH images. Domains whose diameter is significantly larger are expected to produce two filaments in the SH images corresponding to their two boundaries in the X plane.

5 Interpretation of the second-harmonic microscopy contrast and discussion

The SH images of all samples show a bright, approximately uniform signal when the focal plane of the microscope's laser beam coincides with the surface of the sample. In order to understand this effect, we calculated the SH power in the backward direction for a single-domain X -cut sample, using equations from Boyd and Kleinman [35]. The paraxial approximation used there is not fulfilled with good accuracy, but is sufficient for our purpose. Also, we neglected possible changes of the nonlinear tensor near the surface. Note that for a backward-propagating SH wave, the wavenumber mismatch is $\Delta k = k_{\text{SH}} + 2k_{\text{F}}$, with k_{F} the wavenumber of the fundamental light, and not $\Delta k = k_{\text{SH}} - 2k_{\text{F}}$. Therefore, the coherence length of this process is only ≈ 43 nm, much smaller than the Rayleigh length of this beam (250 nm in air) despite of strong focusing. This leads to a very small conversion efficiency in the order of 5×10^{-10} for a peak power of 1 kW at the sample in the case that the focal plane of the beam coincides with the sample surface, and much less otherwise, just as observed in the experiment. The calculated axial and lateral FWHM of this signal are 800 nm and 250 nm, respectively. The axial FWHM can be directly compared with the experimental result [(1 000 ± 200) nm]. Similar to the case of two-photon fluorescence microscopy (Sect. 2), the theoretical resolution tends to be slightly superior as compared with the experimental result, which is, however, reasonable.

The good visibility of the domain walls is surprising. Electric charges at domain boundaries could be visible through the electro-optic effect, if the detection were polarization sensitive, but we obtained our images without a polarizer in the detection system. Also, the observed structures are not modified by heating the samples to 500 °C where the increased ionic conductivity would lead to a compensation of the electric charges at the domain boundaries. A similar argument seems to exclude the effect of mechanical stress as an explanation for the visibility of the filaments: most likely, stress is the origin of the structures at the border of sample C shown in Fig. 4a, but these structures disappeared almost completely when the sample was heated to 700 °C. In contrast, the filaments were influenced only marginally at 700 °C. Therefore we suggest a somewhat speculative explanation (which is unfortunately difficult to check) as follows:

The domain walls may have a certain roughness that can be modelled by a random distribution of light-emitting centres (excited by the pump wave to radiate at the SH frequency), superimposed to a smooth domain boundary which alone would not generate an SH signal. The very short coherence length for radiation in the backward direction (43 nm,

see above) together with the random distribution causes these centres to radiate incoherently (i.e. with random phases). Thus, we have the same situation as in a two-photon fluorescence microscope where the emitted intensities (not the amplitudes) of all centres add up to the detected signal. Contributions from near the focus position dominate the SH signal because the conversion efficiency is greatest at points of high pump intensity. The resolution of the SH microscope determined experimentally for the signal from the filaments [(1 800 ± 200) nm axially, (400 ± 100) nm laterally] can be directly compared with the theoretical resolution calculated for the two-photon fluorescence microscope (1370 nm axially, 250 nm laterally, see Sect. 2). Again, the theoretical performance is somewhat better, which is not surprising.

The situation is slightly different for radiation in the forward direction: here the coherence length is in the order of the Rayleigh length (few microns) so that contributions from light-emitting centres within the focus add up coherently while the (weaker) contributions from outside the focus have different phases. It is also possible that a part of the forward-radiated light is backward scattered at the rough domain walls and contributes to the SH signal measured in the reflected-light mode of the SH microscope. Another explanation for the higher SH efficiency at the domain boundaries could be a different susceptibility $\chi^{(2)}$ of the walls as compared with that for the homogeneous bulk material. More information on the origin of the signal and on the nonlinear optical properties of the walls can be obtained from a future systematic study of the SH intensity and polarization as a function of the crystal orientation and fundamental polarization.

6 Conclusion

We have obtained images of domain structures in periodically poled LiNbO₃ samples, using a scanning SH microscope with a mode-locked laser. Resolutions of 400 nm laterally and a few μm axially have been achieved with this versatile, reproducible, quick and non-destructive technique, which will be useful for the further development of periodically poled waveguide and bulk devices.

Acknowledgements. We wish to thank the Volkswagen Foundation, the Federal Ministry for Science and Research of Northrhine-Westfalia, and the German Federal Ministry for Education, Science, and Research for financial support.

References

1. *Photorefractive Materials and Their Applications II, Survey of Applications*, ed. by P. Günter, J.-P. Huignard, Vol. 62 of Topics in Appl. Phys. (Springer, Berlin, Heidelberg 1989)
2. K. Buse: Appl. Phys. B **64**, 273 (1997)
3. M.M. Fejer: Phys. Today **47**, 25 (1994)
4. M.M. Fejer, G.A. Magel, D.H. Jundt, R.L. Byer: IEEE J. Quantum Electron. **QE-28**, 2631 (1992)
5. G.A. Magel, M.M. Fejer, R.C. Byer: Appl. Phys. Lett. **56**, 108 (1990)
6. M. Yamada, N. Nada, M. Saitoh, K. Watanabe: Appl. Phys. Lett. **62**, 435 (1993)
7. K. Mizuuchi, K. Yamamoto: Appl. Phys. Lett. **66**, 2943 (1995)
8. Q. Chen, W.P. Risk: Electron. Lett. **30**, 1516 (1994)
9. N. Ohnishi, T. Iizuka: J. Appl. Phys. **46**, 1063 (1975)

10. J. Webjörn: *J. Lightwave Technol.* **11**, 589 (1993)
11. K. Distler, L.A. Shenyavskaya: *Krist. Technol.* **11**, 4 (1976)
12. F. Saurenbach, B.D. Terris: *Appl. Phys. Lett.* **56**, 1703 (1990)
13. R. Lüthi, H. Haefke, K.-P. Meyer, E. Meyer, L. Howald, H.-J. Güntherodt: *J. Appl. Phys.* **74**, 7461 (1993)
14. L. Eng, M. Friedrich, J. Fousek, P. Günter: *J. Vac. Sci. Technol. B* **14**, 1191 (1996)
15. R. Le Bihan: *Ferroelectrics* **97**, 19 (1989)
16. G. Rosenman, A. Skliar, I. Lareah, N. Angert, M. Tseitlin, M. Roth: *Phys. Rev. B* **54**, 6222 (1996)
17. Z.W. Hutt, P.A. Thomas, J. Webjörn: *J. Phys. D: Appl. Phys.* **28**, A 189 (1995)
18. F. Kahmann, R. Matull, R.A. Rupp, J. Seglins: *Europhys. Lett.* **13**, 405 (1990)
19. St. MacCormack, J. Feinberg: *Appl. Opt.* **35**, 5961 (1996)
20. V. Grubsky, St. MacCormack, J. Feinberg: *Opt. Lett.* **21**, 6 (1996)
21. S. Kurimura, Y. Uesu: *J. Appl. Phys.* **81**, 369 (1997)
22. Y.R. Shen: *Nature* **337**, 519 (1989)
23. M. Flörsheimer, M. Bösch, Ch. Brillert, M. Wierschem, H. Fuchs: *Adv. Mater.* **9**, 1063 (1997)
24. M. Flörsheimer, H. Salmen, M. Bösch, Ch. Brillert, M. Wierschem, H. Fuchs: *Adv. Mater.* **9**, 1056 (1997)
25. M. Flörsheimer, R. Paschotta, Ch. Brillert, D. Hofmann, W. Sohler, H. Fuchs: unpublished results
26. W. Denk, J.H. Strickler, W.W. Webb: *Science* **248**, 73 (1990)
27. S.W. Hell (Guest Editor): *Bioimaging* **4** (1996), Special Issue on Non-linear Opt. Microsc., pp. 121–224
28. J.B. Pawley: *Handbook of Biological Confocal Microscopy*, 2nd edn. (Plenum Press, New York, London 1995) especially pp. 445–458
29. T. Wilson, C.J.R. Sheppard: *Theory and Practice of Scanning Optical Microscopy* (Academic Press, London 1984) pp. 196–209
30. I. Freund, M. Deutsch, A. Sprecher: *Biophys. J.* **50**, 693 (1986)
31. J.N. Gannaway, C.J.R. Sheppard: *Opt. Quantum Electron.* **10**, 435 (1978)
32. P.E. Hänninen, S.W. Hell: *Bioimaging* **2**, 117 (1994)
33. U. Kubitscheck, M. Tschödrich-Rotter, P. Wedekind, R. Peters: *J. Microsc.* **182**, 225 (1996)
34. S. Hell, G. Reiner, C. Cremer, E.H.K. Stelzer: *J. Microsc.* **169**, 391 (1993)
35. G.D. Boyd, D.A. Kleinman: *J. Appl. Phys.* **39**, 3597 (1968)